

Feasibility of Aerodynamic Flap Hinge Moment Measurements as Input for Load Alleviation Control

Tim Behrens¹

Vestas Wind Systems A/S
Global Research
tibeh@vestas.com

Wei Jun Zhu

Technical University of Denmark
Mechanical Engineering, Fluid Mechanics
wjz@mek.dtu.dk

¹Corresponding author: Frederiksborgvej 399, Building 419, 4000 Roskilde, Denmark

Abstract:

This paper reports a feasibility study on flap hinge moments as sensor input for load alleviation control on smart wind turbine rotors. We designed a controller that used an indicial response method to predict the flap hinge moment assuming constant inflow. The controller compared the predicted with a measured hinge moment in disturbed inflow. The difference of the two values defined a flap deflection set point.

To study the controller's performance, we carried out two-dimensional flow simulations with an unsteady incompressible Reynolds averaged Navier-Stokes code. We investigated a NACA63-200 type airfoil with a trailing edge flap of 16% chord length at a Reynolds number of $Re=10^6$.

The results showed a reduction in lift coefficient variance, compared to the uncontrolled simulation, of 71.76% for a pitch oscillation amplitude of two degrees at a reduced frequency of $k=0.1$. For an amplitude of one degree and a reduced frequency of $k=0.033$ the controller could reduce the variance of the lift coefficient by 83.40%. The maximum flap deflection was four degrees in both directions. To prove the robustness of the control concept, we assessed the individual impacts of signal-to-noise ratio, first order sensor lag, incorrect flow velocity estimation, and increased angle of attack.

We concluded that using the hinge moment as an input for load alleviation control was feasible.

Keywords: smart rotor, load alleviation, trailing edge flap, hinge moment, immersed boundary method

1 Introduction

For future generations of wind turbines, the use of smart rotor systems with distributed aerodynamic actuators is a promising way to reduce loads. In [1], the authors present a summary of the research in smart rotors for wind energy and rotorcraft applications. On wind turbines, smart rotor technologies may lead to a highly reduced cost of energy (through e.g. bigger rotor diameters, closer turbine spacing or placement in complex terrains). The literature provides an insight into different active aerodynamic devices for load alleviation. For use on wind turbines, micro-tabs [2] and trailing edge flaps are the most popular devices. In [3] the authors investigated the aeroelastic response of an elastically mounted airfoil with a deflectable trailing edge. They used a potential flow solver [4] and a linear spring/damper model, concluding significant potential for load reduction. In [5], the author showed that smoothly curved (flexible) flap geometries are beneficial for reductions in airfoil noise and drag.

For a Risø-B1-18 airfoil section equipped with an active trailing edge flap, references [6, 7] present wind tunnel measurements and demonstrate lift amplitude reductions.

An experiment on a small-scale non-rotating blade in a wind tunnel [8] validated the concept of trailing edge flaps for load alleviation under small pitch oscillations. The controller used measurements of the flap-wise bending load. The authors show up to 90% of load variance reductions for feed forward cases. In a following wind tunnel experiment [9], the authors demonstrated load variance reductions in the order of 90% on a rotating two bladed

1.8m diameter scale model. At full-scale, a system demonstrator test on a Vestas V27 turbine [10] delivered first results.

For wind turbines equipped with active aerodynamic control surfaces, local flow sensing becomes a crucial topic. The author of [11] used blade root bending moments as well as local accelerations to derive total blade loads and tip deflections in simulations. In [12], an approach using strain gauge measurements at different span-wise positions demonstrates fatigue load reductions in the blade root bending moment. Full-scale experiments further used Pitot tubes, hot wire anemometers or pressure tabs for local measurements [10, 13].

A disadvantage of most sensor concepts is their low survivability (including frequent replacement of strain gauges, contamination of pressure holes, and lightning attraction). Clearly, integration of the whole flap system into a commercial product is nontrivial and additional restrictions to the blade's structural design and production process should be minimal. In aeronautic research, some studies used the hinge moments of actuator surfaces in control applications. One example includes a model intended as a backup system for inertial measurement units in precision weaponry [14]. The authors made use of the control fins' steady hinge moments, which they derived by computational fluid dynamics (CFD). Additionally, they used external tracking sources for the ammunition flight state. To improve failure detection (e.g. actuator failure or loss of area), [15] used a measurement based polynomial fitting approach for the flap hinge moment. In rotorcraft research, [16] presented an approach for adaptive cancellation of periodic inflow disturbances based on a linear aerodynamic flap model. The authors assumed perfect lift sensing.

A new idea to alleviate loads on wind turbines is to sense the local loading by measuring the fluctuating hinge moment acting upon a trailing edge flap [17]. This measurement can provide an estimate of the change in local loading. The approach requires no extra parts outside the blade structure and may use robust hinge moment sensors. It is beneficial to use an already present trailing edge flap structure to supply a sensor input, especially when considering a possible modular layout of the system. The main difficulty in using the

hinge moment as a sensor input lies in its strong dependence on flap deflection and deflection rate.

Within the present work, we developed a load alleviation controller based on flap hinge moment- and deflection-sensing. We applied the controller to two-dimensional CFD simulations of an airfoil with a flexible trailing edge flap. To investigate feasibility of the approach, we studied the potential reduction of the lift coefficient variance for disturbed inflow conditions. Further, we investigated the robustness of the controller.

2 Numerical methods

To carry out the simulations, we used the incompressible flow solver EllipSys2D developed at Technical University of Denmark (DTU) and Risø-DTU National Laboratory for Sustainable Energy [18, 19, 20]. The code applied domain decomposition and multi-grid methods to solve the incompressible governing equations. This work focused on the two dimensional unsteady Reynolds averaged Navier-Stokes equations (URANS). The chosen turbulence closure was a $k-\omega$ SST model [21]. We integrated an immersed boundary method into the flow solver to represent deflecting trailing edge flaps [22]. Immersed boundary methods model the flow boundaries by adding forcing terms to the governing equations rather than using body conformal grids [23].

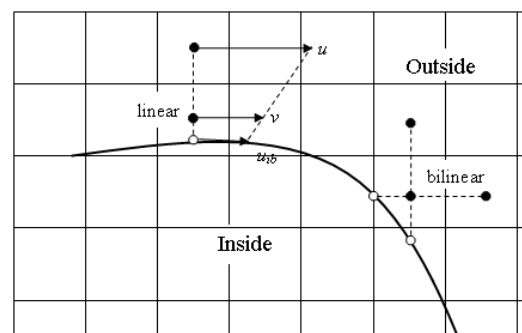


Figure 1: Interpolation scheme. Computational grid (thin —), immersed boundary (—), velocity (\rightarrow), forcing node (\circ), cell centre node (\bullet), and interpolated velocity (v)

The implemented version used a direct one-point forcing approach. The method applied a forcing term to the first

neighboring cell outside the immersed boundary (Figure 1). To find the appropriate velocity it used linear or bilinear interpolation.

We applied a hybrid method, where we modeled the main part of the airfoil in a conventional body-fitted grid and the trailing-edge flap as an immersed boundary.

To generate changing inflow conditions we combined two different methods. The first method was a rotating frame of reference resulting in an added acceleration term \mathbf{a} in the Navier-Stokes equations [24]. This approach allowed simulating a pitching airfoil. An upstream turbulence plane introduced velocity fluctuations via an additional forcing term [25]. We used the turbulence model of Mann [26, 27] to generate the underlying turbulence field.

Equation 1 shows how the combined body forces \mathbf{f} and the rotational acceleration term \mathbf{a} fit into the momentum equation (with fluid density ρ_f , flow velocity \mathbf{V} , pressure p , and dynamic viscosity μ).

$$\rho_f \cdot \frac{D\mathbf{V}}{Dt} = -\nabla p + \mu \nabla^2 \mathbf{V} + \mathbf{f} + \mathbf{a} \quad (1)$$

$$\mathbf{f}^{l+1/2} = -RHS^{l+1/2} + \frac{v^{n+1} - v^n}{\Delta t} \quad (2)$$

Equation 2 shows how the forcing term is calculated. The notation RHS stands for the convective terms, viscous terms and pressure-gradient terms. The notation $l+1/2$ means that the forcing terms were computed before computing the velocity but at the same time step.

3 Modeling of the unsteady hinge moment

For attached flows, aerodynamic indicial response theory [28, 29] deals with solutions to step changes between two steady conditions. The main advantage of this theory is that one can easily compose an arbitrary history of flow state values by single impulse solutions. In general, airfoil loads consist of a circulatory and a non-circulatory term. The circulatory load gradually builds up to a steady value, while the non-circulatory load or 'apparent mass' represents an instantaneous loading that quickly dies out. Hariharan derived an

inviscous compressible flow model for airfoils equipped with plain trailing edge flaps [30]. The model supplies the unsteady additional lift, moment, and hinge moment coefficients for time varying inputs of flap deflection δ and deflection rate $d\delta/dt$. The time-discrete formulation of the model is beneficial for embedded control systems.

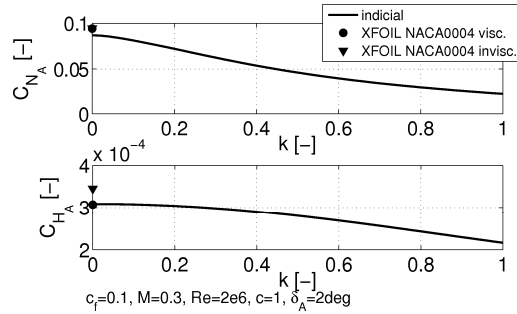


Figure 2: Hariharan [30] model, C_N , and C_H over reduced frequency k , comparison with static XFOIL values of a NACA0004

Figure 2 shows the resulting amplitudes of the main aerodynamic components for a sweep of reduced flap oscillation frequencies. Equation 3 defines the reduced frequency k , where f is the significant frequency; c is the airfoil chord length and V the free stream velocity.

$$k = \frac{\pi f c}{V} \quad (3)$$

The flap length was 10% of the chord and the deflection amplitude was two degrees. For a reduced frequency $k=0$ (i.e. static values) XFOIL calculations of a NACA0012 in viscous and inviscid flow were compared. The difference between the two hinge-moment coefficients is about 10%, while the result of the indicial model lies in between.

Since we used the model in connection with smoothly curved flaps, instead of plain flaps, we investigated the influences of the shape deviation. The displacement in x- and y-direction of each point p for a flap deflection δ was calculated according to equations 4, with S being the distance between flap hinge point (index h) and the trailing edge (index TE). Figure 3 depicts the geometric difference between a plain flap (flap deflection exponent $sc=1$) and a smoothly curved flap ($sc=2$). We defined the flap deflection δ as the negative angle between the line $h-TE$ and the original

chord line. Consequently, the local trailing edge angle for $sc=2$ was higher than the flap deflection angle δ .

$$\Delta x_p = S \cdot \cos(\delta) \cdot [(x_p - x_h)/(x_{TE} - x_h)]^{sc} \quad (4)$$

$$\Delta y_p = S \cdot \sin(\delta) \cdot [(y_p - y_h)/(y_{TE} - y_h)]^{sc}$$

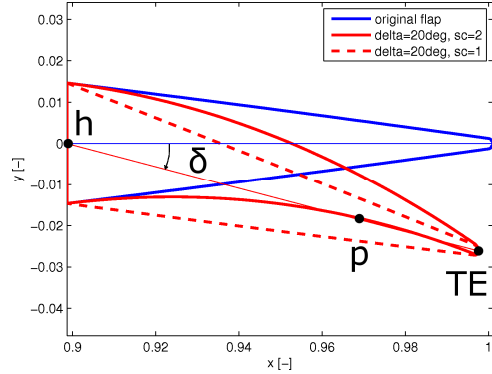


Figure 3: Flap deflection exponent sc

We compared the implemented model with EllipSys2D and Gaunaa's thin airfoil flow model [4]. The latter is able to handle generalized deflection mode shapes (including both plain and smooth flaps). The flow conditions for the comparison were Reynolds number $Re=10^6$, angle of attack $\alpha=0^\circ$, reduced frequency $k=0.1$, and flap length 16% chord. For the EllipSys2D calculations, we used a NACA63-200 geometry (see details in section 5).

Figure 4 shows the amplitudes of the hinge moment coefficient C_h for different oscillating flap deflections. For the plain flap ($sc=1$), the differences between both thin airfoil codes and the EllipSys2D simulations were 40%-60%. Whereas the amplitudes of the plain flap calculated with the Gaunaa code and the curved flap with EllipSys2D agreed well. Gaunaa's code overpredicted the effect of a smoothly curved flap by up to a factor of 3.4 compared with the EllipSys2D results (data not shown). This difference was most likely due to the high trailing edge angle compared to the flap deflection (factor 3.9). In potential flow solvers, the trailing edge angle is of central importance.

Figure 5 presents EllipSys2D results for a pitching airfoil (pitch amplitude $\Phi_A=5^\circ$) at a low reduced frequency of $k=0.01$. For different static flap deflections, the hinge moment coefficients demonstrated a non-linear behavior. The figure also shows that

evaluation of any measured hinge-moment needed information about the flap deflection.

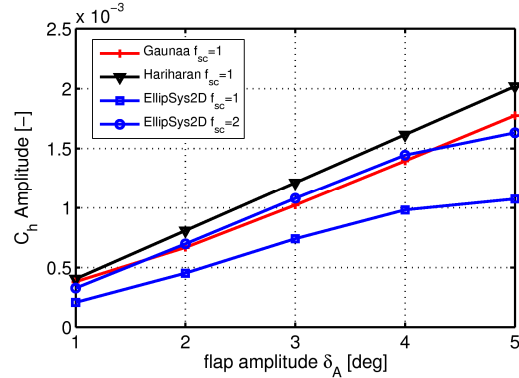


Figure 4: Hinge moment amplitudes for an oscillating trailing edge flap

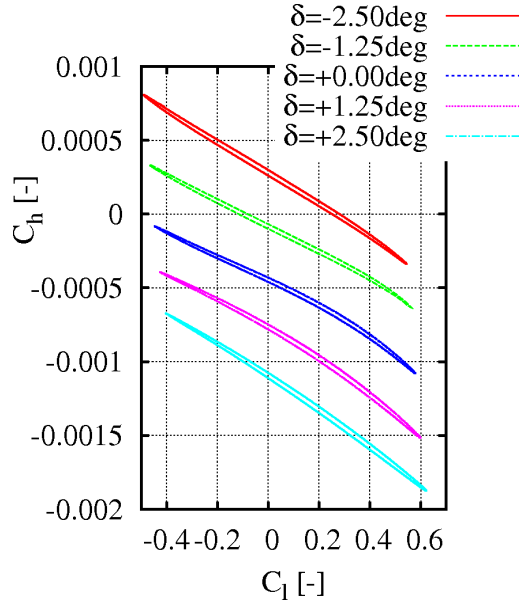


Figure 5: Hinge moment over lift coefficient for a pitching NACA63-216 at $Re=10^6$, different static flap deflections

We introduced flap efficiency factors to manage the viscous effects as well as the shape derivation between the flexible flap and the plain flap. We implemented two additional factors $\varepsilon_{u/d}$ for upward and downward deflections. They were inherent to the used airfoil/flap geometry, but changed with angle of attack and flap deflection. Although a multivariable function $\varepsilon_{u/d}(\alpha, \delta)$ was considered beneficial, we used one static combination of flap efficiency factors to reduce complexity of the design process.

4 Controller design

The implemented controller (see Figure 6) consisted of two parts. The first part was an open-loop control based on the difference between a measured (CFD) and a predicted hinge moment $\Delta C_h = C_h - C_{h,p}$. The predicted hinge-moment coefficient itself consisted of the airfoil's steady state coefficient C_{h0} and the additional part due to the flap deflection. The open-loop provided a flap deflection set-point δ_s . In this investigation, we applied a constant gain $k_h = 4.66 \cdot 10^2$. A low-level PID controller ensured that the flap followed the set point. Additionally, the low-level controller mimicked a real flap actuator by applying restrictions to maximum flap deflection and maximum actuation speed. Further, the updated flap deflection speed was low-pass filtered ($\tau = 2.4\text{ms}$)¹. The results were smoothed flap actuation and an additional flap actuation time constant of $\tau = 3.4\text{ms}$ (for $\Delta\delta = 1^\circ$). For the integral part of the low-level controller, we implemented an anti-windup technique to allow for actuator saturation.

We found the flap efficiency factors by running oscillating flap cases with steady inflow. Additionally, we subjected these coefficients to a parameter optimization for the design control case.

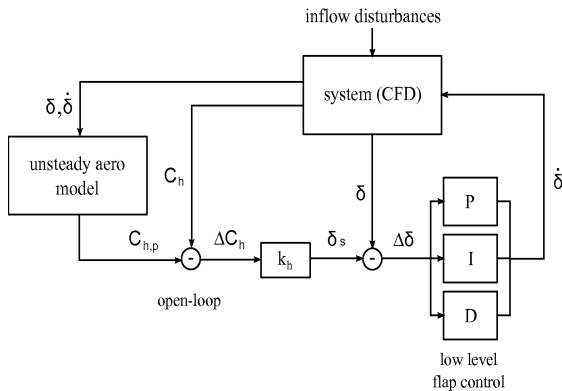


Figure 6: Controller diagram

5 Setup

The airfoil geometry we used was a NACA63-200 with a slightly modified trailing edge and relative thickness of 16.6%. The flap length was 16% of the

chord. We used a hybrid approach when generating the 2D computational domain (Figure 7). For the stationary part of the airfoil, we generated a conventional body conformal C-like grid. We modeled the trailing edge flap as an immersed boundary, moving inside a block attached to the end of the cut airfoil body. We thickened the trailing edge to 0.2% chord since the immersed boundary method needed at least one computational cell inside the body geometry.

The total number of grid points was $64 \cdot 64 \cdot 9 = 36.864$. We set the first cell height above the wall to obtain a dimensionless wall distance y^+ smaller than one. We kept a similar grid spacing close to the immersed boundary.

All calculations were performed at a Reynolds number of $Re = 10^6$. The distance of the airfoil to the free stream boundaries was 11 chord lengths. The one-dimensional turbulence intensity in free stream direction was $TI = 11.85\%$. The simulations ran for 120.000 non-dimensional time steps ($\Delta t = 0.002$), starting from a steady solution. For post-processing the first 5% of the resulting output were dropped, resulting in 7.25 periods of simulated pitch oscillation for $k = 0.1$.

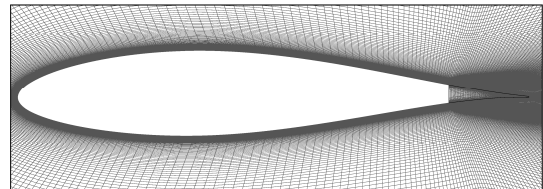


Figure 7: Close-up on the computational mesh immersed boundary (thick —)

6 Results

For the above setup, we investigated different pitch amplitudes and two different reduced frequencies $k = 0.1$ and $k = 0.033$ (corresponding to the 1P and 3P frequencies on a small utility-scale turbine). The maximum allowed flap deflection was fixed to $|\delta_{max}| = 4^\circ$. This gave an estimated maximum change in the equivalent angle of attack of $\alpha_o = \pm 1.6^\circ$ (for a symmetric airfoil, according to [28]).

6.1 Design case

The controller was designed for a pitch amplitude of $\Phi_A = 2^\circ$ at a reduced

¹ All time constants are presented dimensional for a flow velocity of $V = 50\text{m/s}$, and a chord length of $c = 0.6\text{m}$

frequency of $k=0.1$. The baseline angle of attack was $\alpha_c=0^\circ$. Fluctuations from the turbulence plane accounted for an additional angle of attack amplitude of about $\pm 0.5^\circ$. Therefore, the flap could not fully cancel out the effect of the inflow change on C_l . The actuator was saturated a considerable amount of time. We chose the variance σ^2 of the lift coefficient as an estimate of fatigue loads. Equation 5 defines the reduction ρ of the reference variance (uncontrolled).

$$\rho = \frac{\sigma^2}{\sigma_{\text{ref}}^2} \quad (5)$$

For the controlled design case $\rho=71.76\%$ was achieved. The same controller gave $\rho=83.40\%$ for an amplitude of $\Phi_A=1^\circ$ and $k=0.033$. For the combination of pitch amplitude $\Phi_A=1^\circ$ and $k=0.1$ a reduction of $\rho=79.94\%$ was achieved.

Figure 8 shows the relative variance reductions ρ/ρ_0 . The index 0 denotes the C_l variance reduction of 83.40% for the best case ($k=0.033$, $\Phi_A=1^\circ$). The drop at $\Phi_A=0.5^\circ$ was due to the pitch oscillation effect being in the order of the stochastic turbulence fluctuation, as indicated by the values of the absolute variances. For zero pitch amplitude, the controller even increased the variance since only high frequency disturbances were present.

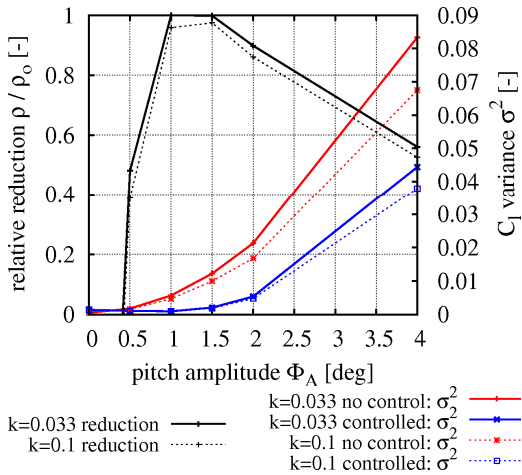


Figure 8: Relative variance reductions

6.2 Robustness

For wind turbine implementation of the hinge-moment based controller, we considered the rotor speed and flap deflection to be measurable with good

quality. The wind speed estimate by nacelle anemometers was considered less suited for high-speed control purposes. The uncertainty of hinge moment measurements is depending on the chosen sensor type and setup.

We investigated the effect of signal noise, first order sensor time constant, and estimated total inflow velocity on the relative reduction ρ/ρ_0 . The index 0 denotes the reduction for the design case ($k=0.1$, $\Phi_A=2^\circ$).

To investigate changes in signal-to-noise ratio (SNR), we added white Gaussian

$$SNR(dB) = 20 \cdot \log\left(\frac{A_s}{A_n}\right) \quad (6)$$

noise to the hinge moment measurement. Equation 6 defined the SNR in decibel; A_s and A_n were the amplitudes of the signal and the added noise respectively. Figure 9 depicts the results, showing the raw SNR and the input to the controller after low-pass filtering with a time constant of $\tau=0.3ms$. Low-pass filtering naturally enhanced the results when signal noise was present. For a SNR of 3dB, ρ/ρ_0 dropped to around 70%.

To investigate the effect of signal lag, we changed the time constant of a first order sensor model. As shown in Figure 10, increasing the time constant decreased the potential for load reduction. At $\tau=0.044s$ the relative reduction dropped to 50%, while at $\tau=0.077s$ no load reduction was achieved.

The dimensionless force and moment coefficients are by definition directly affected by changes in air density and flow velocity. For a small utility-scale wind turbine, we assumed the wind speed estimate to be off by $\pm 5\%$. The resulting uncertainty in the airfoil's inflow velocity would be around $\pm 0.35\%$. Figure 11 shows the behavior of the relative reduction ρ/ρ_0 , when we modified the value of the flow velocity V within both the hinge moment model and the calculation of the hinge moment coefficient. An error of $\pm 5\%$ on the flow velocity V estimate resulted in a ρ/ρ_0 of 85% for the lower estimate and a decrease to 69% for the higher estimate. Increasing the velocity estimate by 10%, we could no longer achieve a significant load reduction, while decreasing the

estimate by 10% lowered the relative reduction to 56%.

We applied the controller to a range of angles of attack α_c . For each angle of attack, we adjusted the corresponding steady $C_{H0,2}$. Figure 12 shows the C_l variances σ^2 and the relative reductions ρ/ρ_0 based on the design case. The controller operated above 94% of relative reduction ρ/ρ_0 for $0^\circ < \alpha_c < 9.5^\circ$. Further increase in angle of attack resulted in a steep drop in ρ/ρ_0 .

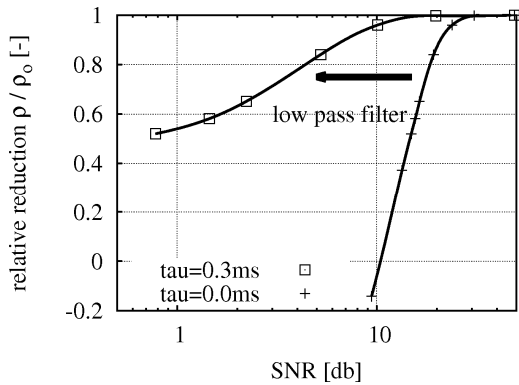


Figure 9: Variation of signal-to-noise ratio

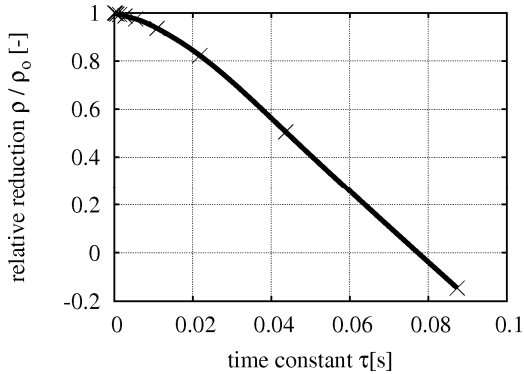


Figure 10: Variation of first order model time constant τ

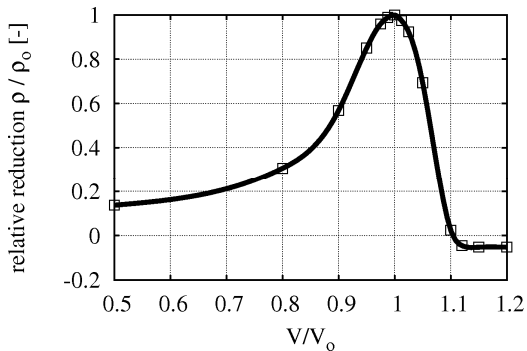


Figure 11: Variation of estimated inflow velocity V

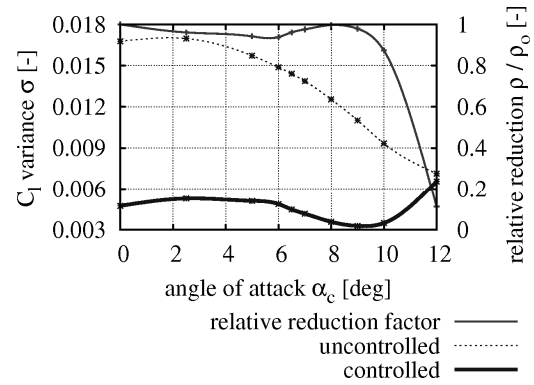


Figure 12: Variances of lift coefficient over center angle of attack α_c .

7 Conclusions

We used the hinge moment of a trailing edge flap as sensor input for load alleviation control. A thin airfoil model based on indicial response theory predicted the flap hinge moment in steady inflow for arbitrary flap deflections. The controller compared this predicted hinge moment with a measurement. Based on the difference, the controller generated a flap deflection set point aiming to reduce fluctuations in lift coefficient. We applied the controller to CFD simulations of an airfoil with a flap of 16% chord length. The inflow disturbances consisted of a rotating frame of reference and an additional turbulence plane upstream of the airfoil.

We showed that the hinge-moment based control could alleviate the effect of inflow disturbances, even with frequently saturated actuators. The reduction in lift coefficient variance was 71.76% for the design case of underlying pitch oscillation amplitude $\Phi_A=2^\circ$ at a reduced frequency of $k=0.1$. For an amplitude of $\Phi_A=1^\circ$ and a reduced frequency of $k=0.033$, a maximum reduction in C_l variance of 83.40% was demonstrated.

Both a SNR of 3dB and a first order model time constant of 30ms each resulted in a decrease to 70% of the maximum variance reduction. Erroneous flow velocity estimation of -5% decreased the reduction to 85%, while overestimating by 5% resulted in 69% of maximum variance reduction. The controller operated above 93% of relative reduction ρ/ρ_0 for $0^\circ < \alpha_c < 9.5^\circ$.

Despite the rather small flap deflections of only four degrees, the developed

alleviation method showed fair potential and was comparable to a controller using the deviation in lift coefficient as control error (data not shown). Flap configurations with more control authority might lead to better results. For the presented method, longer flaps with moderate deflections would be beneficial to enhance the signal quality and reduce the risk of separation. Enhanced prediction of the hinge-moment, by additional stall modeling in the potential flow model (as e.g. in [32]) or implementing parameterized flap efficiency factors, might further improve the results. The integration of more advanced control schemes like model predictive control and system identification might be beneficial, although the higher computational effort might pose a problem to application in embedded controls.

We concluded that using the hinge moment as input for load alleviation control was feasible.

Acknowledgment

The authors acknowledge the Danish National Advanced Technology Foundation (Højteknologifonden) for support.

References

1. Barlas TK and van Kuik GAM. Review of state of the art in smart rotor control research for wind turbines. *Prog Aerospace Sci*, 2009
2. van Dam CP et al. Computational Investigations of Small Deploying Tabs and Flaps for Aerodynamic Load Control. *J. Physics: Conf. Ser. 75 012027*, 2007
3. Buhl T and Gaunaa M. Potential Load Reduction Using Airfoils with Variable Trailing Edge Geometry. *J. Sol. Energy Eng. November 2005, Volume 127, Issue 4*, 2005
4. Gaunaa M. Unsteady 2D Potential-flow Forces on a Variable Geometry Airfoil Undergoing Arbitrary Motion. Technical report, Risø-R-147, 2005
5. Trolborg N. *Computational Study of the Risø-B1-18 Airfoil equipped with actively controlled Trailing Edge Flaps*. MSc thesis at Technical University of Denmark, Fluid Mechanics Section, 2004
6. Bak C et al. Wind tunnel test on airfoil Risø-B1-18 with an Active Trailing Edge Flap. *Wind Energy 13:207–219*, 2010
7. Andersen PB. Advanced load alleviation for wind turbines using adaptive trailing edge flaps: sensing and control. Risø PhD Report, Ph.D. thesis, case number: 274-05-0398, 2010
8. van Wingerden J-W et al. On the Proof of Concept of a ‘Smart’ Wind Turbine Rotor Blade for Load Alleviation. *Wind Energ. 2008; 11:265–280*, 2008
9. van Wingerden J-W et al. Two-Degree-of-Freedom Active Vibration Control of a Prototyped “Smart” Rotor. *Control Systems Technology, IEEE Transactions on*, vol.PP, no.99, pp.1-13, 2010
10. Castaignet D et al. Results from the first full scale wind turbine equipped with trailing edge flaps. 28th AIAA Applied Aerodynamics Conference, 28 June - 1 July 2010, Chicago, Illinois, AIAA 2010-4407, 2010
11. Abdallah I. *Advanced load alleviation for wind turbines using adaptive trailing edge geometry: Sensing techniques*. MSc thesis, Technical University of Denmark, 2006
12. Andersen PB et al. Deformable Trailing Edge Flaps for Modern Mega-Watt Wind Turbine Controllers using Strain Gauge Sensors. *Wind Energy 13:193–206*, 2010
13. Madsen HA et al. The DAN-AERO MW Experiments. Final report. Technical Report, Risø DTU, National Laboratory for Sustainable Energy, Risø-R-1726(EN)., September 2010
14. Ratliff R and Pagilla P. Fault tolerant robust flight control using surface actuator hinge moments. In *American Control Conference, June 2008*, pp. 1612–1617, 2008.
15. Gross HN, Chandler PR, and Eslinger RA. Renewed interest in hinge moment models for failure detection and isolation. In *American Control Conference Proceedings, 18-20 June 1986*, pp. 1497–1502, 1986
16. Ariyur K and Krstic M. Feedback attenuation and adaptive cancellation of blade vortex interaction noise on a helicopter blade element, In *American Control Conference, 1998*.

- Proceedings, Volume 2, 1053 –1057, 1998.*
17. Abdallah I et al. Wind turbine blade and method for controlling the load on a blade. World Intellectual Property Organization, Pub. No.: WO/2009/056136, 2009.
 18. Michelsen JA. Basis3D - a platform for development of multiblock PDE solvers. Technical Report AFM 92-05, Technical University of Denmark, 1992.
 19. Michelsen JA. Block structured multigrid solution of 2D and 3D elliptic PDEs. Technical Report, AFM 94-06, Technical University of Denmark, 1994.
 20. Sørensen NN. General Purpose Flow Solver Applied to Flow over Hills. PhD thesis, Risø National Laboratory, 1995.
 21. Sørensen NN. k-omega turbulence models implementation and testing. Technical Report Risø Report R-864, Risø National Laboratory, 1995.
 22. Behrens T et al. Calculations of Flow around an Airfoil with a Trailing Edge Flap by Use of an Immersed Boundary Method. *European Wind Energy Conference and Exhibition Proceedings*, 2009
 23. Mittal R and Iaccarino G. Immersed boundary methods. *Annu. Rev. Fluid Mech.*, 37(1):239–, 2005.
 24. White FM. *Viscous fluid flow*. McGraw-Hill, Inc., 1991
 25. Troldborg N, Sørensen JN, Mikkelsen R. Actuator Line Simulation of Wake of Wind Turbine Operating in Turbulent Inflow. *J. Physics: Conf. Ser.* 75 012063, 2007
 26. Mann J. The spatial structure of neutral atmospheric surface-layer turbulence. *Journal of Fluid Mechanics*, 273(-1):141–168, 1994.
 27. Mann J. Wind field simulation. *Probabilistic Engineering Mechanics*, 13(4):269 – 282, 1998.
 28. Theodorsen T. General theory of aerodynamic instability and the mechanism of flutter. Technical Report 496, NACA, 1935.
 29. Wagner H. Über die Entstehung des dynamischen Auftriebes von Tragflügeln. *Zeitschrift für angewandte Mathematik und Mechanik*, 5(1):17-35, 1925.
 30. Hariharan N. *Unsteady aerodynamics of a flapped airfoil in subsonic flow using indicial concepts*. Master's thesis, Dept. of Aerospace Engineering, University of Maryland, 1995.
 31. Abbott H and von Doenhoff AE. *Theory of Wing Sections*. Dover publications, Inc. New York, 1959
 32. Andersen PB, Gaunaa M, Bak C and Hansen MH. A dynamic stall model for airfoils with deformable trailing edges. *Wind Energy*, 12:734–751, 2009